Isomer-Specific Spectroscopy and Conformational Isomerization Energetics of *o*-, *m*-, and *p*-Ethynylstyrenes

Talitha M. Selby,[†] Jasper R. Clarkson,[†] Diane Mitchell,[‡] James A. J. Fitzpatrick,[‡] Hsiupu D. Lee,[†] David W. Pratt,*[,‡] and Timothy S. Zwier*[,†]

Department of Chemistry, Purdue University, West Lafayette, Indiana 47907-2084, and Department of Chemistry, University of Pittsburgh, Pittsburgh, Pennsylvania 15260

Received: February 18, 2005; In Final Form: March 31, 2005

The infrared and ultraviolet spectroscopy of *o*-, *m*-, and *p*-ethynylstyrene isomers (*o*ES, *m*ES, and *p*ES) were studied by a combination of methods, including resonance-enhanced two-photon ionization (R2PI), UV−UV hole-burning spectroscopy (UVHB), resonant ion−dip infrared spectroscopy (RIDIRS), and rotationally resolved fluorescence excitation spectroscopy. In addition, the newly developed method of stimulated emission pumping−population transfer spectroscopy (SEP-PTS) was used to determine the energy threshold to conformational isomerization in *m*-ethynylstyrene. The $S_1 \leftarrow S_0$ origin transitions of *o*ES and *p*ES occur at 32 369 and 33 407 cm^{-1}, respectively. In *m*ES, the *cis* and *trans* conformations are calculated to be close in energy. In the R2PI spectrum of *m*ES, the two most prominent peaks (32672 and 32926 cm^{-1}) were confirmed by UVHB spectroscopy to be $S_1 \leftarrow S_0$ origins of these two conformers. The red-shifted conformer was identified as the *cis* structure by least-squares fitting of the rotationally resolved fluorescence excitation spectrum of the origin band. There are also two possible conformations in *o*ES, but transitions due to only one were observed experimentally, as confirmed by UVHB spectroscopy. Density functional theory calculations (B3LYP/6-31+G*) predict that the *cis-ortho* conformer, in which the substituents point toward each other, is about 8 kJ/mol higher in energy than the *trans-ortho* isomer, and should only be about 5% of the room temperature population of *o*ES. Ground-state infrared spectra in the C−H stretch region (3000−3300 cm^{-1}) of each isomer were obtained with RIDIRS. In all three structural isomers, the acetylenic C−H stretch fundamental was split by Fermi resonance. Infrared spectra were also recorded in the excited electronic state, using a UV−IR−UV version of RIDIR spectroscopy. In all three isomers the acetylenic C−H stretch fundamental was unshifted from the ground state, but no Fermi resonance was seen. The first observed and last unobserved transitions in the SEP-PT spectrum were used to place lower and upper bounds on the barrier to *cis* → *trans* isomerization in *m*-ethynylstyrene of 990−1070 cm^{-1}. Arguments are given for the lack of a kinetic shift in the measurement. The analogous *trans* → *cis* barrier is in the same range (989−1065 cm^{-1}), indicating that the relative energies of the zero-point levels of the two isomers are $(E_{ZPL}(cis) - E_{ZPL}(trans)) = -75$ to $+81$ cm^{-1}. Both the barrier heights and relative energies of the minima are close to those determined by DFT (Becke3LYP/6-31+G*) calculations.

I. Introduction

Substituted benzenes are recognized to play an important role in the pathways to larger polyaromatic hydrocarbons (PAHs) in combustion engines and more generally in flames.[1,2] The chemical complexity of many of the substituted aromatics in fuels and fuel-rich flames necessarily opens the possibility for structural and conformational isomers. One anticipates that different structural isomers could have substantially different chemical reactivity, particularly in their abilities to form larger PAH molecules. The same can be said for conformational isomers, where conformational isomerization may need to precede structural isomerization by bringing the ring-forming segments of the molecule into close proximity to one another. The need for combustion models to include structural and conformational isomers has long been recognized,[3−6] but now these models are pushing deeper into the processes leading to soot formation, requiring explicit consideration of isomers of substituted aromatics.[7,8]

The structural isomers of ethynylstyrene (*o*-, *m*-, and *p*-) are intriguing candidates for isomer-specific characterization. Besides the three structural isomers, both *ortho*- and *meta*-isomers should also possess two conformational isomers associated with the different orientations of the vinyl group relative to the acetylenic substituent (*cis* and *trans*).

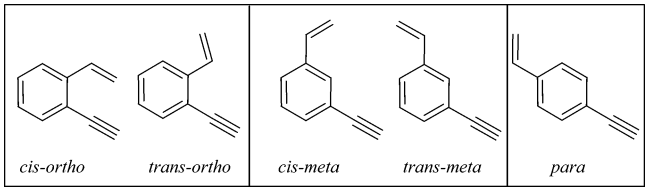

Since ethynylstyrene shares the same molecular formula ($C_{10}H_8$) as naphthalene, in principle any of these isomers could undergo unimolecular isomerization to naphthalene. However,

* Corresponding authors. E-mail: zwier@purdue.edu. Phone: (765) 494-5278. Fax: (765) 494-5330. E-mail: pratt@pitt.edu. Phone: (412) 624-8660. Fax: (412) 624-8611.
[†] Purdue University.
[‡] University of Pittsburgh.

10.1021/jp050858g CCC: $30.25
Published on Web 05/03/2005

facile ring-closing would seem likely only in the *cis-o*-ethynylstyrene isomer. The ground-state pathway from *cis-o*ES to naphthalene has been explored theoretically by Hopf and coworkers.[9] The first step toward exploring isomer-specific reactivity is to characterize the ultraviolet and infrared spectroscopy of each of the isomers. This is the primary task of the present study.

The electronic structure of these isomers is also intriguing. The presence of two conjugated substituents on the phenyl ring raises the issue of whether the first excited state will involve both substituents equally or favor one over the other. Furthermore, if both substituents are involved in the electronic excitation, the interaction of the two substituents could produce transition moments, normal modes, and Franck−Condon activity quite different from either singly substituted species.

There are also practical issues remaining to be addressed from a previous photochemistry study from our group.[10] Two of the $C_{10}H_8$ products from the reaction of metastable diacetylene (C_4H_2*) with styrene were identified by previous one-color R2PI studies as *m*-ethynylstyrene and 1-phenyl-1-butene-3-yne. However, at the time, samples of the other $C_{10}H_8$ isomers were not available to us, and it seemed mysterious that only one of the three possible ethynylstyrene isomers was formed in the reaction. We therefore decided to synthesize all three isomers and carry out a more complete characterization of their spectroscopy, including searches for conformational isomers. As we shall see, this search held some surprises, including the necessity for reassigning the observed product in the C_4H_2* + styrene reaction.

Finally, armed with the results of the isomer-specific spectroscopy, it is possible to use the unique infrared or ultraviolet transitions of a particular structural and/or conformational isomer to initiate isomer-specific unimolecular or bimolecular photochemistry. In that spirit, we have employed stimulated emission pumping (SEP) to selectively excite single conformations of *m*-ethynylstyrene (*m*ES), thereby initiating conformational isomerization. The newly developed method of SEP-population transfer spectroscopy[11] has then been used to determine the energy thresholds to cis-trans and trans-cis isomerization of *m*ES. These thresholds compare favorably with the fitted form of the vinyl group's torsional potential in styrene, based on observed progressions in the torsional mode in the single vibronic level fluorescence spectra.[12]

II. Experimental Details

The detailed syntheses of all three *x*-ethynylstyrenes ($x = 2$, 3, 4) and their analysis data are provided in the Supporting Information. Briefly, 1-ethenyl-*x*-trimethylsilylethynylbenzenes were first synthesized following the palladium-catalyzed coupling procedures[13−16] of the commercially available *x*-bromostyrenes and trimethylsilyl acetylene with minor modification. The following procedure is representative. Dichlorobis(triphenylphosphine)palladium(II) and copper(I) oxide were added to an *x*-bromostyrene in piperidine at room temperature under nitrogen. After the suspension was stirred for 2 h, trimethylsilylacetylene was added. The mixture was heated and stirred at 50−52 °C until completion. After completion, the reaction mixture was cooled. The precipitate was removed by filtration and washed with hexane. Water was added to the filtrate, and the mixture was extracted with hexane. The combined extract was dried (Na_2SO_4), filtrated, and concentrated to give a black, oily residue. Distillation of the residue gave a colorless liquid, which was further purified by flash chromatography (hexane).

x-Ethynylstyrenes were prepared by removing the trimethylsilyl group from 1-ethenyl-*x*-trimethylsilylethynylbenzenes with potassium fluoride[17,18] in DMSO. The following procedure is representative. Potassium fluoride (15 equiv) was added to a 1-ethenyl-*x*-trimethylsilylethynylbenzene in DMSO, and the suspension was stirred at room temperature for 4 h. Hexane was added, and the organic layer was extensively washed with water, dried (Na_2SO_4), and concentrated. The concentrated residue was purified by flash chromatography (hexane), which afforded the desired *x*-ethynylstyrene.

Most of the experiments described in this paper were carried out on a molecular beam time-of-flight mass spectrometer at Purdue, which has been described previously.[19] Briefly, the molecular beam was produced by passing He over a sample reservoir heated to about 50 °C. A total pressure of 2 bar was applied behind a pulsed valve (Jordan Co.) with a 0.8 mm diameter orifice.

In resonance-enhanced two-photon ionization (R2PI) experiments, the $S_1 \leftarrow S_0$ transition was excited with the frequency doubled output of an Nd:YAG pumped tunable dye laser operating at 20 Hz (0.2 mJ/pulse). For *p*ES, one-color R2PI could be carried out. However in *m*ES and *o*ES, a more energetic photon was needed to reach the ionization potential from the S_1 state. In this case, 266-nm light was used from the fourth harmonic of a second Nd:YAG laser. The power of the 266-nm light was kept low (*ca.* 0.1 mJ/pulse) because it introduced a background one-color R2PI signal that was temporally coincident with the desired two-color ion signal. Ions produced were accelerated into the TOF mass spectrometer and detected by a microchannel plate ion detector. The ion signals were amplified 25 times (Stanford Research System Model SR445) and then signal averaged by a fast digital oscilloscope (Tektronix Model 3025B). Signal averaging was controlled by Lab View software. The pulsed valve and laser(s) timing were controlled with an eight-channel pulse delay generator (Berkley Nucleonic Model 555).

Conformer specific ultraviolet spectra were recorded with ultraviolet hole-burning (UVHB) spectroscopy. In UVHB experiments a second tunable dye laser operating at 10 Hz was fixed at a particular $S_1 \leftarrow S_0$ transition in the R2PI spectrum. The power of this hole-burn laser (0.4 mJ/pulse) was sufficient to partially saturate the transition. A probe R2PI laser followed and interrogated the same molecules 20−50 ns later. The probe laser (20 Hz) was tuned across the $S_1 \leftarrow S_0$ vibronic transitions of interest. When the probe laser was resonant with a transition that shared the same ground state as the transition where the holeburn laser was set, depletion in the ground-state population was detected by the probe laser. The difference between the ion signal with and without the holeburn laser present was monitored *via* active baseline subtraction with a gated integrator.

Conformer-specific infrared spectra were recorded with resonant ion dip infrared spectroscopy (RIDIRS). In this technique,[20] a tunable infrared source acted as a hole-burn laser, preceding the ultraviolet laser(s) used for R2PI by 50−200 ns. The R2PI laser's frequency was fixed on a transition out of the ground-state zero-point level of a particular species so that there was constant ion signal, while the IR laser was tuned through the region of interest (3000−3360 cm^{-1}). When the infrared source was resonant with a vibrational transition of the species being monitored, population was removed from the ground-state zero-point level, causing a decrease in the constant ion signal. By detecting the difference in 20 Hz ion signal created by the 10 Hz infrared laser in active baseline subtraction, the ground-state vibrational spectrum was recorded.

Simply by changing the timing of the laser pulses, infrared spectra could be recorded in the S_1 excited state as well.[21] In

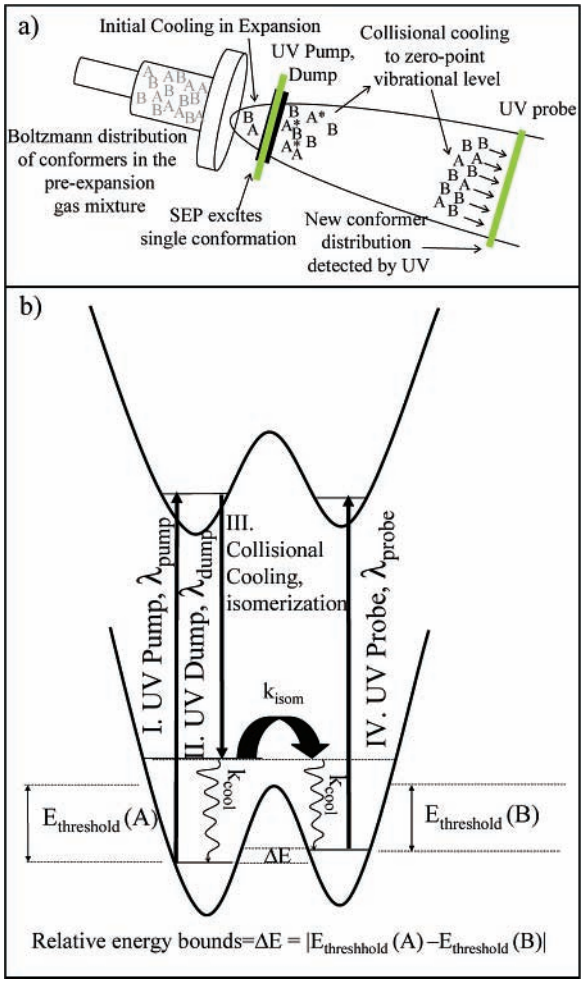

Figure 1. (a) Schematic diagram of the spatial and temporal arrangement and (b) energy-level diagram for the SEP-PT experiment.

this case, the infrared laser pulse occurred 15 ns after the S_0-S_1 UV pulse, but 15 ns prior to the S_1-ion step. When the infrared laser was resonant with an S_1-state infrared transition, fast nonradiative processes brought these molecules into states which could not be ionized efficiently ($T_n(v)$ or $S_0(v)$), leading to a depletion in the ion signal. For RIDIRS experiments, the infrared source was a tunable infrared optical parametric oscillator/optical parametric amplifier pumped by a Continuum 8000 Series seeded Nd:YAG laser. Typical infrared powers used range from 2 to 10 mJ/pulse.

Rotationally resolved fluorescence excitation experiments were performed on a high-resolution apparatus at the University of Pittsburgh, which has been described elsewhere.[22] Briefly, the sample was heated to about 80 °C, seeded in He, expanded through a 240 μm quartz nozzle, collimated with a skimmer, and crossed 10 cm downstream by a frequency doubled tunable CW dye laser, using Kiton Red and Rhodamine 6G dyes. The fluorescence signal was collected with 30% efficiency collection enhancement optics and imaged onto a photomultiplier tube. Absolute frequency calibration was performed by simultaneously recording the iodine absorption spectrum and Etalon frequency markers. The resulting spectra were fit by using the JB95 rotational least-squares fitting program.[23]

Stimulated emission pumping (SEP) experiments of *m*ES were recorded in a laser-induced fluorescence chamber that has been described previously.[11] SEP and SEP-induced population transfer (SEP-PT) experiments are depicted schematically in Figure 1. SEP experiments[11] were performed with the pump laser (λ_{pump}, 20 Hz, 0.1 mJ/pulse) fixed on the $S_1 \leftarrow S_0$ origin transition. Stimulated emission back to the ground state was accomplished by a second tunable laser (λ_{dump}, 10 Hz, 0.3 mJ/pulse) delayed from the pump by 5−20 ns, a time scale short compared to the measured S_1 lifetime (80 ns). When resonant with a ground-state vibration, the depopulation in the excited state caused depletion in the total fluorescence signal observed. The difference in the fluorescence signal was recorded as a function of the dump laser frequency, using active baseline subtraction.

In SEP-PT experiments,[11] the SEP step was performed following initial cooling in the expansion in the collisional region of the expansion 2 mm from the exit of a 1-mm-diameter nozzle (i.e., $x/D = 2$). Following the SEP excitation of a specific conformer, the excited conformer could either cool back down to its zero-point level or, if its energy is above the barrier to isomerization, a fraction of the excited conformational population could isomerize and then be collisionally cooled to the product's zero-point level. By monitoring the fluorescence signal from a third probe laser (λ_{probe}, 0.1 mJ, 20 Hz, positioned at $x/D = 6$) fixed on the origin transition of the product conformer, an increase in population of that conformer will be observed whenever the dump laser encounters a transition with sufficient energy to isomerize to the monitored conformation. The resulting SEP-PT spectrum can then be compared to the SEP spectrum as a function of dump laser wavelength, plotted as energy above the excited conformer's zero-point level, to determine the isomerization efficiency. The first transition observed in the SEP-PT spectrum constitutes a firm upper bound on the energy barrier to isomerization. The last unobserved transition places a lower bound on the barrier if there is no kinetic shift in the measurement, that is, if the isomerization rate is sufficiently fast at threshold to compete successfully with collisional cooling back into the reactant well. Since the A → B and B → A thresholds probe the same barrier, the difference in thresholds places bounds on the relative energies of the A and B minima, that is,

$$\Delta E = E_{ZPL}(B) - E_{ZPL}(A) = E_{thresh}(A \rightarrow B) - E_{thresh}(B \rightarrow A) \quad (1)$$

Thus, within certain constraints, the SEP-PT data are capable of providing direct measurements of the energies of key stationary points on the potential energy surface for isomerization, the relative energies of the minima, and the barrier separating them.

Density functional theory (DFT) calculations with a Becke-3LYP[24,25] functional and the 6-31+G*[26] basis set were used to determine structures, energies, and harmonic vibrational frequencies. True minima were verified by the lack of imaginary frequencies in the harmonic vibrational frequency calculations. Transition-state structures were optimized at the Becke3LYP/6-31+G* level employing the QST3[27] algorithm. Configuration interaction single (CIS)[28] calculations with a 6-31G basis set were performed to obtain predictions for the excited-state rotational constants and transition dipole moments. DFT and CIS computations were carried out with Gaussian 98.[29]

III. Overview of the Spectroscopy of Related Mono- and Disubstituted Benzenes

The ultraviolet and infrared spectroscopy presented in this work builds off of a significant body of previous work on similar systems, including styrene,[30−33] phenylacetylene,[32,34] and the diethynylbenzene[21,35] and divinylbenzene[36] isomers. The relevant

aspects of this work are briefly summarized here for easy comparison with the ethynylstyrene spectra.

In styrene, the vibronic structure present in the S_0-S_1 transition is dominated by progressions involving ring elongation modes ($6a^1_0$ and 13^1_0 in benzene, at 394 and 1209 cm^{-1}, respectively) and the ring breathing modes (1^1_0 and 12^1_0 in benzene, at 746 and 948 cm^{-1}, respectively).[30] In addition, several low-frequency vibronic bands in the 230−350 cm^{-1} region have been assigned to even overtones and combination bands involving out-of-plane vibrations of the vinyl group. Dispersed fluorescence from these bands has been used to determine the shape of the potential for the phenyl−vinyl torsion (ν_{42} in styrene) in the ground electronic state.[31] The torsional potential is very floppy about the planar configuration, with a fundamental frequency of only 38 cm^{-1} and a torsional barrier of ~1000 cm^{-1}. In the excited state, the $\pi-\pi^*$ excitation increases the double bond character of the ring-vinyl C−C bond, thereby raising the torsional frequency to ~150 cm^{-1}. Duschinsky mixing of the torsion with out-of-plane bending modes spreads the torsional Franck−Condon intensity in the excitation spectrum over several $n + m = 2$ bands in the 230−350 cm^{-1} region. Similar vibronic structure is observed in a series of fluorostyrenes and methylstyrenes.[37−42]

Phenylacetylene, with its linear ethynyl substituent, lacks the torsional coordinate of styrene. As a result, the low-frequency vibronic transitions due to torsion are absent. In their place, phenylacetylene has several b_2-symmetry fundamentals (e.g., 142, 492 cm^{-1}) which appear due to vibronic coupling with the $S_2(^1A_1)$ state.[34] These serve as false origins for progressions involving the same totally symmetric vibrations of the phenyl ring as in benzene and styrene ($6a^1_0$, 1^1_0, 12^1_0,). The vibronic spectroscopy of *o*-, *m*-, and *p*-diethynylbenzene is similar to that of phenylacetylene, but with varying degrees of vibronic coupling to S_2.[21]

Several of the S_0-S_1 origin transitions of these singly and doubly substituted benzenes have been studied at high resolution.[32,36] From the fitted ground and excited state rotational constants, it is possible to surmise the key structural changes that accompany electronic excitation. In addition, the fitting determines the direction of the transition moment, which depends sensitively on the nature and relative position of the substituents. The results of these determinations are summarized in Figure 2a,b for styrene,[32] phenylacetylene,[32] and three isomers of divinylbenzene[36] studied in previous work. The analogous tentative deductions of transition moment directions in the S_0-S_1 transitions of the diethynylbenzene isomers are also included (Figure 2d), based on vibronic level arguments.[21] The results in Figure 2 will be used as a point of comparison with the present work.

IV. Results and Analysis

A. R2PI, UVHB, and High-Resolution Fluorescence Excitation Spectra. The R2PI spectra of the three ethynylstyrene structural isomers in the region of the $S_1 \leftarrow S_0$ transition are shown in Figure 3. *p*ES has only one conformation possible, and its $S_1 \leftarrow S_0$ origin is assigned to the furthest red peak at 33 407 cm^{-1}. Two conformations are possible for *o*ES; however, the isomer in which the vinyl group is *trans* relative to the ethynyl substituent is calculated to be lower in energy than the *cis* isomer by 7.45 kJ/mol (8.33 kJ/mol including zero-point energy correction) at the DFT (B3LYP/6-31+G*) level of theory. The UVHB spectrum of *o*ES (not shown), recorded with the hole-burn laser fixed at 32 369 cm^{-1}, confirms that all

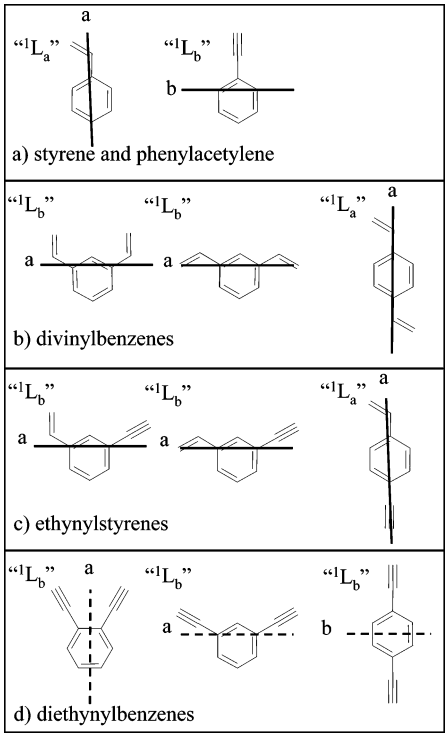

Figure 2. Observed electronic transition dipole moment directions of (a) styrene and phenylacetylene, (b) divinylbenzenes, (c) ethynylstyrenes, and (d) diethynylbenzenes (see text for discussion).

observed transitions arise from the same ground-state level, so that all observed transitions can be assigned to *trans-o*ES. The origin of *trans-o*ES is thus assigned to the furthest red transition at 32 369 cm^{-1}.

In *m*ES, the two most prominent peaks occur with about equal intensity at 32 672 and 32 926 cm^{-1}. The UVHB spectra (Figure 4b,c) of *m*ES show that these transitions are due to different species and are thus assigned to the two conformational isomers of *m*ES. The two origins occur with about equal intensity, consistent with the predictions of the DFT (B3LYP/6-31+G*) calculations, which show that the *cis* isomer is only 0.10 kJ/mol above the *trans* conformer (0.33 with ZPE correction).

To make firm conformational assignments and to probe the structures and transition moments more directly, rotationally resolved fluorescence excitation spectra were recorded for *p*ES and conformer A of *m*ES. Attempts were made to record the analogous spectrum of conformer B of *m*ES, but insufficient sample was available for success in this endeavor.

Figure 5 shows the rotationally resolved fluorescence excitation spectrum of the 0^0_0 band of *p*ES. An expanded region of the P-branch is shown below the overview spectrum, together with the best fit from the analysis. The standard deviation of the fit of 100 transitions is 4.6 MHz. Figure 6 shows the rotationally resolved fluorescence excitation spectrum of the 0^0_0 band of *m*ES(A) along with the best fit in an expanded portion of the R-branch shown in the two bottom traces. The standard deviation of the fit of 110 transitions is 3.6 MHz. The line shape of each transition in the *p*ES and *m*ES(A) spectra is dominated by a Voigt profile containing a 44 MHz Doppler-broadened Gaussian component. A small Lorentzian component was held fixed at 2 MHz to be consistent with the 80 ns S_1 lifetime for these molecules. Best-fit rotational constants in S_0 are listed in Table 1, where they are compared with the calculated values from the DFT calculations. The large differences in the calculated ground-state rotational constants of the two *m*ES conformers are sufficient to make a firm conformational

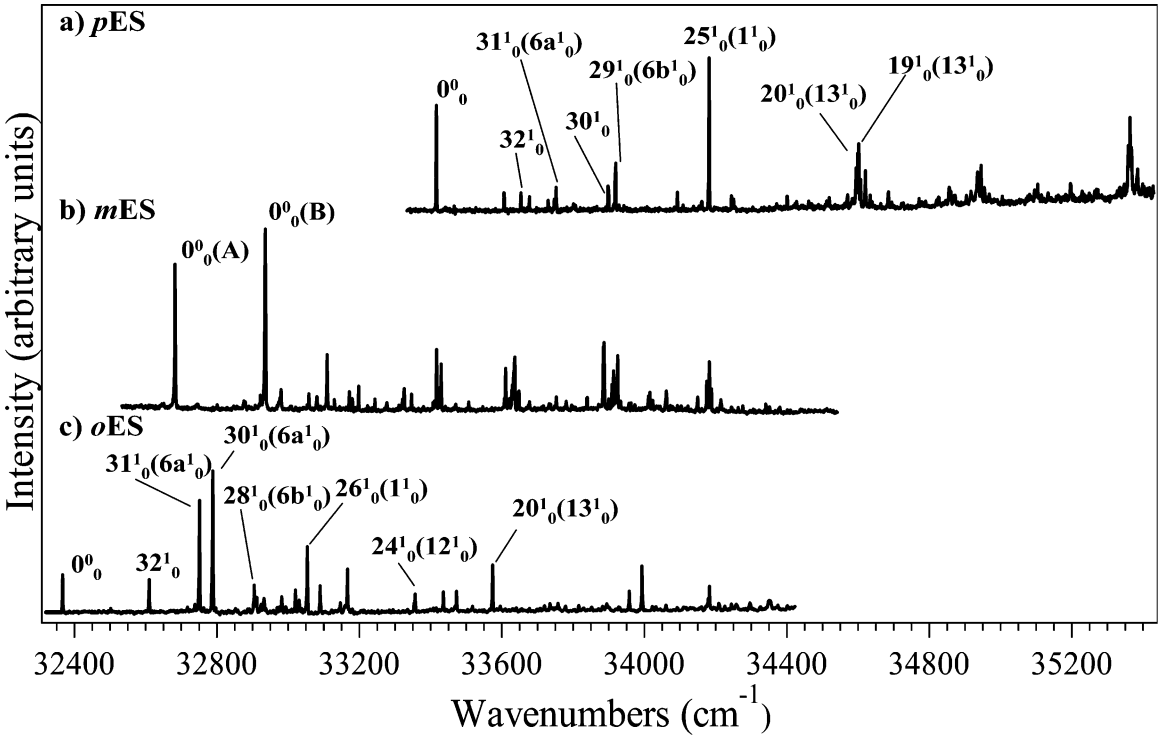

Figure 3. R2PI of (a) *p*-, (b) *m*-, and (c) *o*-ethynylstyrene, showing several tentative assignments for fundamental transitions in *p*- and *o*-ethynylstyrene (see text for discussion).

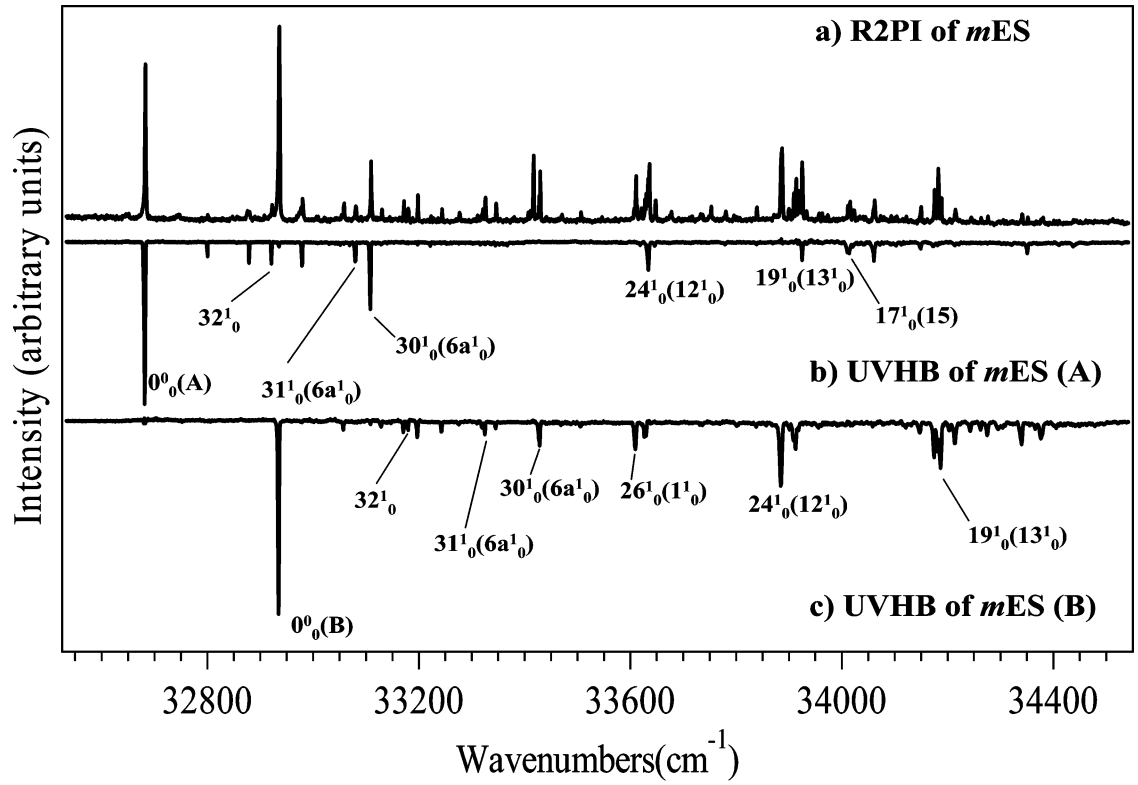

Figure 4. (a) R2PI spectrum of *m*-ethynylstyrene and UVHB spectra of *m*-ethynylstyrene (b) conformer A and (c) conformer B, showing several tentative assignments for fundamental transitions (see text for further discussion).

assignment of *m*ES(A) to the *cis* conformer. By process of elimination, then, *m*ES(B) is assigned to the *trans* conformer. The small inertial defects in the ground and excited states of both *p*ES and *cis*-*m*ES indicate that both molecules are planar in S_0 and S_1 states (see Table 2).

Because of the asymmetry of the vinyl substituent, there are no restrictions on the in-plane direction of the transition moment, which for a $\pi-\pi^*$ transition will be somewhere in the *ab* plane of either molecule. However, in both *p*ES and *m*ES(A) all fitted transitions were *a*-type. A few *b*-type transitions were detected, but the upper bound for the amount of *b* character in transition dipole moments for both *m*ES(A) and *p*ES is only about 15%. Thus, the electronic transition dipole moments in both *cis*-mES and *p*ES lie almost parallel to the *a*-inertial axis (see Figure

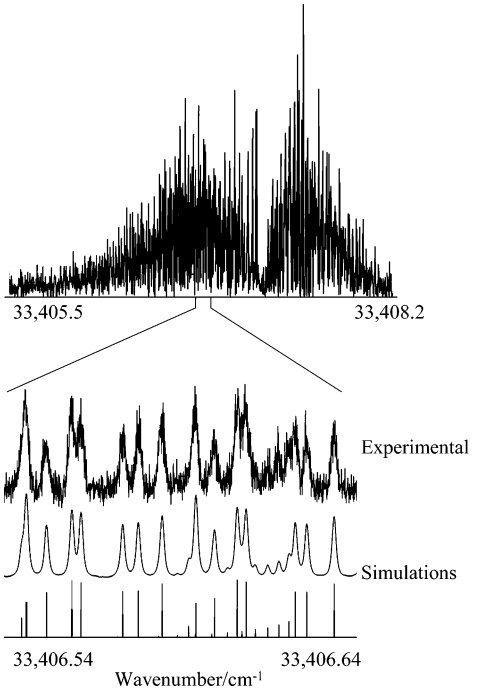

Figure 5. Rotationally resolved fluorescence excitation spectrum of the 0^0_0 band of *p*-ethynylstyrene. The bottom traces show an expanded portion of the P-branch and computer simulations with and without a convoluted line shape function.

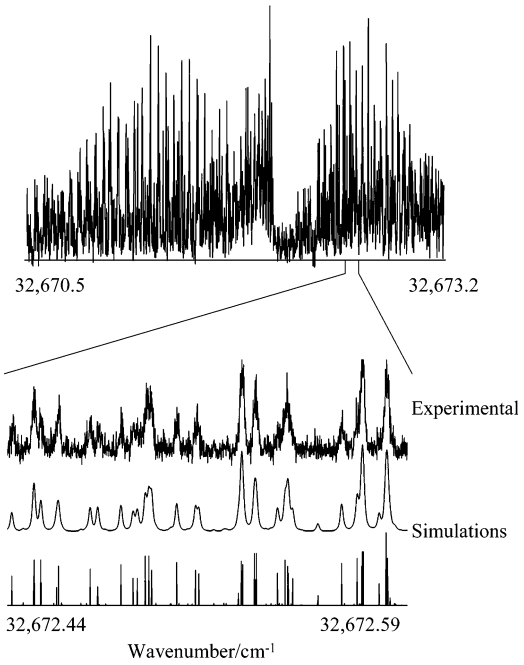

Figure 6. Rotationally resolved fluorescence excitation spectrum of the 0^0_0 band of *m*-ethynylstyrene (A). The bottom traces show an expanded portion of the R-branch and computer simulations with and without a convoluted line shape function.

2c). Furthermore, while a fittable spectrum of *m*ES(B) could not be obtained before sample ran out, it was clear that the band was also primarily *a*-type. We will return to a discussion of transition moments in Section V. It is worth noting here that the ethynylstyrene isomers have S_0-S_1 transition moment directions that closely parallel those of the corresponding isomers of divinylbenzene (compare parts b and c in Figure 2).

The high-resolution spectra have led to a firm conformational assignment of the bands in the R2PI and UVHB spectra of *m*-ethynylstyrene. As a result, we now turn attention to the

TABLE 1: Comparison of Experimental Rotational Constants of *p*ES and *m*ES(A) with Calculated Rotational Constants of the Four Ethynylstyrene Isomers in the Ground Electronic States at the DFT (B3LYP/6-31+G*) Level of Theory

Calculated				
parameter	*p*ES	*cis*-*m*ES	*trans*-*m*ES	*trans*-*o*ES
A'' (MHz)	5009.5	2252.2	3027.1	1609.2
B'' (MHz)	703.3	973.4	833.2	1458.3
C'' (MHz)	616.7	679.7	653.4	765

Experimental		
parameter	*p*ES	*m*ES(A)
A' (MHz)	5030(2)	2261(2)
B' (MHz)	709.2(2)	982.6(2)
C' (MHz)	621.5(2)	685.2(2)

TABLE 2: Experimentally Determined Rotational Parameters of *p*ES and *m*ES(A) in Their Ground and Excited Electronic States

parameter	*p*ES	*m*ES(A)
A'' (MHz)	5030(2)	2261(2)
B'' (MHz)	709.2(2)	982.6(2)
B'' (MHz)	709.2(2)	982.6(2)
B'' (MHz)	709.2(2)	982.6(2)
C'' (MHz)	621.5(2)	685.2(2)
κ''	−0.96	−0.62
$\Delta I''$ (amu Å^2)	0.1(2)	−0.1(2)
A' (MHz)	4847(2)	2217(2)
B' (MHz)	705.7(2)	979.4(2)
C' (MHz)	615.6(2)	679.1(2)
κ'	−0.96	−0.61
$\Delta I'$ (amu Å^2)	0.5(3)	0.3(2)
OMC (MHz)	4.6	3.6
fwhm (MHz)	46	46
band type	*a*/*b* hybrid	*a*/*b* hybrid

vibronic structure present in the R2PI and UVHB spectra of the four observed isomers of ES. In what follows, the Mulliken numbering scheme[43] will be used to label the observed bands. However, when vibrational modes bear strong resemblances to those in benzene or monosubstituted benzenes, the Wilson scheme[44] will be included in parentheses. Recall that, in the latter numbering scheme, ν_1, ν_6, ν_{12}, and ν_{13} display prominent Franck−Condon progressions in most substituted benzenes. Because of the asymmetry of the vinyl substituent, all the isomers of ES are of C_s symmetry, making all in-plane vibrational fundamentals symmetry allowed. In addition, vibrational modes that are of similar frequency but different symmetry in the C_{2v} benzene derivatives are often mixed in the ethynylstyrene isomers. Without dispersed fluorescence spectra, the assignments are made based on comparisons with previously studied molecules, backed by calculations. Unfortunately, since CIS (6-31G) calculations do not correctly describe the close-lying S_1 and S_2 states, those results cannot serve as a fully reliable guide in making assignments.

1. p-Ethynylstyrene. The FC activity in *p*ES (and all the ethynylstyrenes) is what is expected for a conjugated substituted benzene, that is, most of the FC activity lies in the ring and substituent-sensitive stretching and bending modes. The most intense peak observed in the R2PI spectrum of *p*ES (Figure 3a) occurs 765 cm^{-1} above the origin and is assigned to 25^1_0 (1^1_0), a ring-breathing vibration. The corresponding vibration occurs in *p*-diethynylbenzene[21] (*p*DEB), phenylacetylene[34] (PA), and styrene[30,33] (STY) at 760, 718, and 746 cm^{-1}, respectively. Other prominent features observed in the R2PI spectrum of *p*ES (summarized in Figure 3a and Table 3) are the totally symmetric fundamentals, 19^1_0 (13^1_0), 20^1_0 (13^1_0), 26^1_0 ($6a^1_0$), 29^1_0 ($6b^1_0$),

TABLE 3: Tentative Assignments of the Major Peaks Observed in R2PI of Ethynylstyrenes

	*p*ES frequency (cm^{-1})			*cis-o*ES frequency (cm^{-1})			*trans-m*ES frequency (cm^{-1})			*cis-m*ES frequency (cm^{-1})		
description	exptl[a]	calcd[b]	mode[c]	exptl[a]	calcd[b]	mode[a]	exptl[a]	calcd[b]	mode[c]	exptl[a]	calcd[b]	mode[c]
vinyl/C−C≡CH bends	237	228	32^1_0	243	237	32^1_0	245	232	32^1_0	240	232	32^1_0
x-sensitive bend/stretch	482	482	30^1_0	384	384	31^1_0						
x-sensitive stretch/bend	336	369	31^1_0	421	441	30^1_0	390	397	31^1_0	399	427	31^1_0
x-sensitive stretch/bend	676	660	26^1_0				411	453	30^1_0	426	454	30^1_0
$6b^1_0$ /C−C≡CH bend	503	524	29^1_0	537	559	28^1_0	493	514	29^1_0	538	547	28^1_0
ring breathing	765	791	25^1_0	686	705	26^1_0	674	693	26^1_0			
ring C−C	1182	1183	20^1_0	990	990	24^1_0	950	966	24^1_0	952	968	24^1_0
ring C−C	1185	1184	19^1_0	1207	1183	20^1_0	1252	1213	19^1_0	1243	1209	19^1_0
ring C−C										1330	1297	17^1_0
combination bands	985		$29^1_0 30^1_0$	627		$31^1_0 32^1_0$	802		$30^1_0 31^1_0$	963		$28^1_0 30^1_0$
	1101		$25^1_0 31^1_0$	664		$30^1_0 32^1_0$	904		$29^1_0 30^1_0$	1351		$24^1_0 31^1_0$
	1178		$26^1_0 29^1_0$	800		$30^1_0 31^1_0$	1085		$26^1_0 30^1_0$	1378		$24^1_0 30^1_0$
	1247		$25^1_0 30^1_0$	919		$28^1_0 31^1_0$	1168		$26^1_0 29^1_0$	1492		$24^1_0 28^1_0$
	1268		$25^1_0 29^1_0$	956		$28^1_0 30^1_0$	1341		$24^1_0 31^1_0$	1668		$19^1_0 30^1_0$
	1441		$25^1_0 26^1_0$	1071		$26^1_0 31^1_0$	1362		$24^1_0 30^1_0$	1755		$17^1_0 30^1_0$
	1530		25^2_0	1108		$26^1_0 30^1_0$	1442		$24^1_0 29^1_0$			
	1664		$20^1_0 30^1_0$	1373		$24^1_0 31^1_0$						
	1667		$19^1_0 30^1_0$	1410		$24^1_0 30^1_0$						
	1685		$20^1_0 29^1_0$	1591		$20^1_0 31^1_0$						
	1688		$19^1_0 29^1_0$	1628		$20^1_0 30^1_0$						
	1947		$20^1_0 25^1_0$									
	1950		$19^1_0 25^1_0$									

[a] Experimental frequency, measured from the origin. [b] Ground-state frequency calculated with DFT (B3LYP/6-31+G*) and scaled by 0.9565. [c] Numbering according to Mulliken.[43]

30^1_0, 31^1_0 ($6a^1_0$), and 32^1_0. All these modes also occur in combination with 25^1_0 (1^1_0). The feature at 503 cm^{-1} is assigned to 29^1_0 ($6b^1_0$), a mixed mode that contains both in-plane CC≡CH bending and ring deformation. The corresponding modes in PA[34] and *p*DEB[21] are 35^1_0 and 20^1_0, respectively. In both PA and *p*DEB, this mode is observed at 492 cm^{-1} and acts as a false origin that gains intensity *via* vibronic coupling. 29^1_0 ($6b^1_0$) also occurs in combination with 19^1_0 (13^1_0), 20^1_0 (13^1_0), and 30^1_0. Since both S_1 and S_2 are A′ states, it is possible that vibronic coupling to the S_2 state is affecting the intensities of some of the in-plane fundamentals.

The low-frequency vibrations occurring at 189, 260, 313, 330, and 336 cm^{-1} in *p*ES are left unassigned. Since there is only one unassigned in-plane low-frequency mode left, it follows that most of this activity is due to even overtones and combinations of out-of-plane vibrations. Recall that this is the energy region (230−350 cm^{-1}) where the overtones and combinations of the vinyl torsion and out-of-plane vinyl bends are expected to appear based on styrene (Section III). Assignments of this structure must await single vibronic level fluorescence (SVLF) experiments.

2. trans-o-Ethynylstyrene. Of the three isomers, the origin of *o*ES is weakest (Figure 3c). The peaks with the most intensity occur at 384 and 421 cm^{-1}. No long progressions exist in these modes, and both of these modes act as false origins for other vibronic structure (Table 3). Thus, we assign the 384- and 421-cm^{-1} bands to in-plane vibrational fundamentals that gain intensity *via* vibronic coupling to the S_2 state. CIS (6-31G) calculations predict that the first two excited states are of A′ symmetry with the state having the higher oscillator strength being lower in energy. The observation of strong vibronically induced transitions suggests that the ordering of the states from the CIS calculation is wrong, since the S_2 ($2^1A'$) ← S_0 ($\tilde{X}^1A'$) transition must have a greater oscillator strength than the S_1 ($1^1A'$) ← S_0 ($\tilde{X}^1A'$) transition for intensity stealing to produce vibronic transitions of greater intensity than the S_1 ← S_0 origin.

The two most intense features at 384 and 421 cm^{-1} are assigned to ring-elongation modes which are mixed with side chain bending vibrations to produce 31^1_0 ($6a^1_0$) and 30^1_0 ($6a^1_0$), respectively. The difference between these modes is that ν_{31} is a mixture of ring elongation in the direction of the vinyl group with ethynyl group bending, whereas ν_{30} is the reverse (ethynyl ring elongation and vinyl bend). The substituent bends occur in PA[34] and STY[30,33] at 492 and 437 cm^{-1}, respectively, and the ring elongation in PA[34] and STY[30,33] occurs at 410 and 394 cm^{-1}, respectively. As summarized in Figure 3 and Table 3, other prominent features that are assigned to in-plane fundamentals are 20^1_0 (13^1_0), 24^1_0 (12^1_0), 26^1_0 (1^1_0), 28^1_0 ($6b^1_0$), and 32^1_0. These bands also occur built off 31^1_0 ($6a^1_0$) and 30^1_0 ($6a^1_0$). Unlike *p*ES and *m*ES, there is only one low-frequency vibration in *o*ES, 32^1_0, which is assigned to the vinyl bending vibration.

3. m-Ethynylstyrene. While the vibronic structure of the two meta isomers is similar (Figure 4b,c), there are distinct differences as well. The S_1 ← S_0 origin transitions of both conformations of *m*ES are by far the most intense bands in the spectra (Figure 4b,c). The bands at 950/952 and 1252/1243 cm^{-1} are assigned as the ring modes 19^1_0 (13^1_0) and 24^1_0 (12^1_0) in *trans-m*ES/*cis-m*ES. Besides the origin transitions, the most intense band in the *cis-m*ES spectrum occurs at 426 cm^{-1} and is assigned to 30^1_0 ($6a^1_0$), a substituent-sensitive ring elongation. This mode occurs in PA[34] at 410 cm^{-1} and in *m*DEB[21] at 405 cm^{-1}. In *cis-m*ES, there is no higher member of a 30^n_0 progression, suggesting that 30^1_0 derives much of its intensity from vibronic coupling with the S_2 state. Alternatively, the FC factors for higher members of this progression may be too small to be observed. The corresponding vibration in *trans-m*ES occurs at 411 cm^{-1}, but it is not very intense. Other prominent features in *cis-m*ES are 17^1_0 (15^1_0), 28^1_0 ($6b^1_0$), 31^1_0 ($6a^1_0$), and 32^1_0 (Figure 4b).

Other prominent transitions in *t-m*ES are the bands tentatively assigned as 26^1_0 (1^1_0), 29^1_0 ($6b^1_0$), 31^1_0 ($6a^1_0$), and 32^1_0. Though 31^1_0 ($6a^1_0$), a substituent-sensitive ring-elongation mode, is not extremely intense, it has combination bands occurring with 24^1_0 (12^1_0), 29^1_0 ($6b^1_0$), and 30^1_0 ($6a^1_0$). The band tentatively assigned to 32^1_0, the vinyl bend fundamental, is experimentally observed between 237 and 245 cm^{-1} in the ethynylstyrenes and at 237

TABLE 4: Calculated Frequencies of Modes that May Be Involved in the Ground-State Fermi Resonance of the Ethynylstyrenes in the Acetylenic CH Stretch Region

		calcd freq (cm^{-1})[b]			
mode[a]	description	*o*ES	*p*ES	*trans-m*ES	*cis-m*ES
ν_1	C≡C−H stretch	3332	3334	3333	3332
ν_9	C≡C stretch	2107	2110	2114	2114
ν_{28}	ip C≡C−H bend	620	616	617	618
ν_{42}	oop C≡C−H bend	560	561	565	567
combination bands					
$\nu_9 + \nu_{28} + \nu_{42}$		3287	3287	3296	3299
$\nu_9 + 2*\nu_{28}$		3347	3342	3348	3350
$\nu_9 + 2*\nu_{42}$		3227	3232	3244	3248

[a] Modes in *p*ES. [b] Calculated at the DFT (B3LYP/6-31+G*) level of theory and scaled by 0.9566.

cm^{-1} in STY.[45] Other low-frequency vibronic bands in *cis-m*ES at 119, 197, 298, and 375 cm^{-1} and in *trans-m*ES at 123, 194, 236, 262, and 308 cm^{-1} are left unassigned. As in *p*ES, we believe that many of these transitions are even overtones and combinations of out-of-plane vibrations that involve vinyl torsional motion.

B. Ground and Excited-State RIDIRS Spectra. Figure 7a−d presents the ground electronic state RIDIR spectra of *p*-, *o*-, *cis-m*-, and *trans-m*-ethynylstyrene, respectively. These spectra span the aromatic/vinyl C−H stretch region (3000−3150 cm^{-1}) and acetylenic C−H stretch region (3300−3350 cm^{-1}). The most notable spectroscopic signature in these spectra is the extensive Fermi mixing observed in the acetylenic C−H stretch region. The occurrence of Fermi mixing of the acetylenic CH stretch with one quantum of C≡C stretch and two quanta of C≡C−H bend has been documented for PA[46,47] and the DEBs.[21]

As the spectra of *p*ES and *m*ES(A) show most clearly, the principal Fermi resonance in the acetylenic CH stretch fundamental is with a single state. However, further mixing produces further splitting of the two principal bands into a final set of 3−4 resolved or partially resolved bands.

Table 4 presents the calculated frequencies for the C≡C−H bends, C≡C stretch, and C≡C−H stretch along with the combination bands that may be involved in Fermi resonance with the acetylenic CH stretch. If the computed frequencies are close to the experimental values, then the two likely candidates for mixing with the acetylenic CH stretch are $\nu_9 + 2\nu_{28}$ and $\nu_9 + \nu_{28} + \nu_{42}$. However, without experimental data for the C≡CH bends and C≡C stretch frequencies, it is difficult to make these assignments with confidence.

Figure 8a−d presents the excited electronic state RIDIR spectra of *p*-, *o*-, *cis-m*-, and *trans-m*-ethynylstyrene, respectively. The most notable feature in these spectra is that the extensive Fermi mixing observed in the ground state in the acetylenic C−H stretch fundamental is absent in the excited state. In all cases except *p*ES, only a single peak is observed in this region. These occur at 3320, 3326, and 3325 cm^{-1} for *o*ES, *cis-m*ES, and *trans-m*ES, respectively. *p*ES has one strong transition at 3328 cm^{-1} and a weak transition at 3341 cm^{-1}. This same removal of Fermi resonance in the excited state is also observed in the DEBs and is attributed to the shifting in frequency of the C≡C stretch and C≡C−H bends.[21] In PA, the C≡C stretch is lower by about 100 cm^{-1} in S_1 than in S_0.[34]

C. SEP and SEP-PT Spectra. The SEP and SEP-PT spectra of *m*ES have one primary goal: namely, to measure the energy thresholds for *cis* → *trans* and *trans* → *cis* isomerization. As mentioned in the Introduction, the hole-filling methods developed in our laboratory[11] offer a unique and direct method of measuring the energy thresholds for conformational isomerization. In *m*ES, one anticipates that the barrier height for isomerization will be similar to the C_ϕ-vinyl torsional barrier in styrene (1070 cm^{-1}).[12] This latter barrier was derived from fitting the torsional progression in ν_{42} observed in SVLF spectra of styrene. The torsional potential should correspond closely to the *cis*−*trans* reaction coordinate in *m*ES, although the extent to which motion along other coordinates could modify the isomerization threshold from the pure torsion can be tested from our measurements.

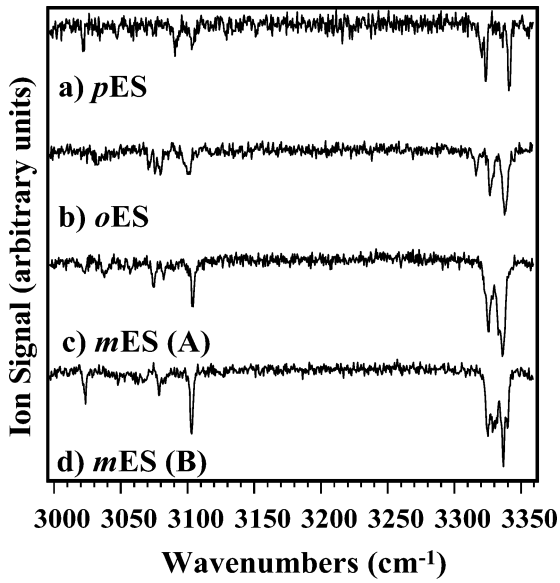

Figure 7. Ground-state RIDIR spectra of (a) *p*-, (b) *o*-, (c) *cis-m*-, and (d) *trans-m*-ethynylstyrene in the CH stretch fundamental region.

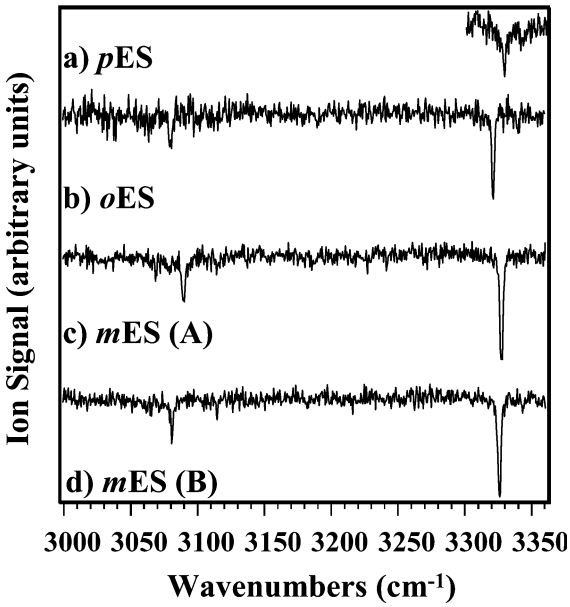

Figure 8. Excited-state RIDIRS of (a) *p*-, (b) *o*-, (c) *cis-m*-, and (d) *trans-m*-ethynylstyrene in the CH stretch fundamental region.

Figure 9a,c presents the SEP spectra of *cis-mES* and *trans-mES*, respectively, with the difference in pump and dump wavelengths plotted as energy above the ground-state zero-point level along the abscissa. The SEP spectra highlight the energy region 900−1400 cm^{-1} where the energy thresholds for isomerization should appear, based on styrene. Not surprisingly, the SEP spectra of *cis-mES* and *trans-mES* are very similar, reflecting large Franck−Condon factors from the S_1 ZPL of

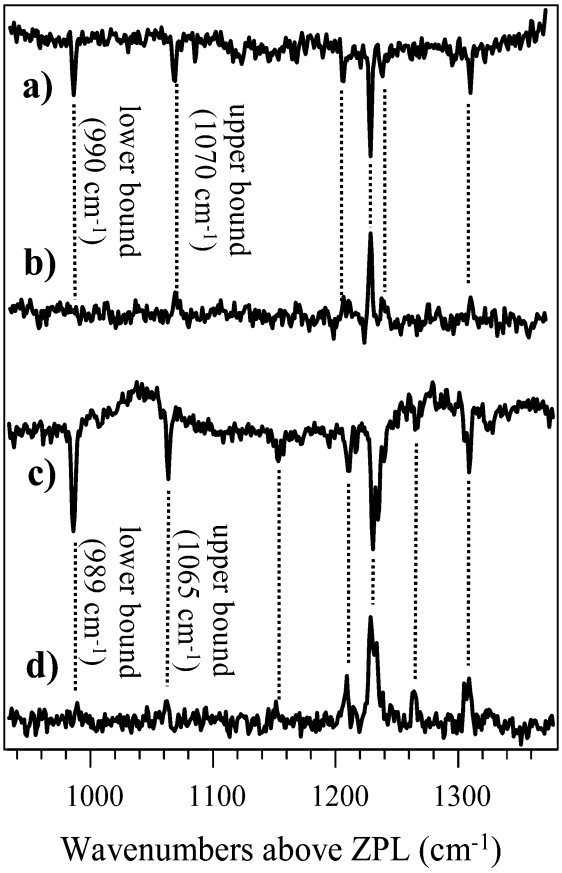

Figure 9. Stimulated emission pumping spectra of (a) *cis-m*ES (*m*ES-(A)) and (c) *trans-m*ES (*m*ES(B)). Stimulated emission pumping population transfer spectra of (b) *cis-m*ES(A) → *trans-m*ES(B) and (d) *trans-m*ES(B) → *cis-m*ES(A).

each isomer to the ring mode fundamentals at 990 and 1230 cm^{-1} (corresponding to 12^0_1 and 13^0_1 in benzene, respectively). For our purposes here, the SEP spectra provide a comparison with the SEP-population transfer spectra below them

In the SEP-PT spectra of *cis-mES* → *trans-mES* (Figure 9b), the pump laser was fixed to the S_0-S_1 origin transition of the *cis-m*ES reactant and the downstream probe laser on the *trans-m*ES product origin transition. Using a 20 Hz/10 Hz/20 Hz pump/dump/probe configuration, the SEP-PT spectrum highlights the difference in population induced in the product by the dump laser. A comparison of the SEP-PT spectrum (Figure 9b) with the SEP spectrum above it (Figure 9a) shows that the strong SEP transition at 990 cm^{-1} is missing, while the corresponding transitions at 1230 and 1309 cm^{-1} are clearly observed. In following the SEP-PT spectrum down from the 1230-cm^{-1} peak, small transitions at 1206 and 1070 cm^{-1} are observed as weak, but clearly reproducible population gains. Since the first observed peak at 1070 cm^{-1} represents an upper bound to the energy barrier to *cis* → *trans* isomerization, clearly establishing its presence is especially important. We have analyzed the signal-to-noise ratio of this band and have determined that its integrated intensity is more than two standard deviations outside the integrated noise level of other regions of the spectrum. Thus, the 1070-cm^{-1} band is present at a 95% confidence limit, and serves as the upper limit for the energy barrier for the *cis* → *trans* isomerization. Since the more intense band at 990 cm^{-1} in the SEP spectrum is missing from the SEP-PT spectrum, it places a lower bound on this energy threshold. The small intensity of the first observed band above threshold must be a result of a competition between isomerization and vibrational cooling right at threshold. We will discuss this further shortly.

Figure 9d presents the SEP-PT spectrum for the isomerization in the reverse direction, namely, the *trans* → *cis* reaction. The SEP-PT spectra in the two directions are nearly identical with one another, with the 1231-cm^{-1} band large, the 1065-cm^{-1} transition present but small, and the 989-cm^{-1} band missing. Similar analysis places the upper bound to the *trans* → *cis* isomerization threshold at 1065 cm^{-1} with 95% confidence limits. By contrast, a careful comparison of the SEP and SEP-PT spectra in the region of the 989-cm^{-1} band indicates that the apparent structure in the SEP-PT spectra is not aligned with the band in the SEP spectrum.

Since the threshold measurements in the two directions probe the same barrier, in combination they place bounds on the relative energies of the two minima, with

$$E(trans) - E(cis) = (E_{thresh} - E(cis)) - (E_{thresh} - E(trans))$$
$$= (990 - 1070) - (989 - 1065) = -75 - 81 \text{ cm}^{-1}$$

Thus, as expected, the two *m*-ES isomers are nearly isoenergetic.

V. Discussion and Conclusions

A. Conformation-Specific Spectroscopy, Conformational Cooling, and Conformational Product Identification. A combination of supersonic expansion cooling and laser-based double resonance spectroscopy have been used to record isomer-specific infrared and ultraviolet spectra of four structural and conformational isomers of ethynylstyrene. Ultraviolet hole-burning spectroscopy determined that both the *cis* and *trans* isomers of *m*ES are present in the expansion, but only the trans conformer is present for *o*ES. The electronic origins of the four isomers are spread over more than 1000 cm^{-1}, making spectroscopic distinction straightforward, especially under jet-cooled conditions. Infrared studies also provided unique spectral signatures of the different isomers, but they were not as useful a diagnostic of the isomers, since the acetylenic and vinylic CH stretch fundamentals show only small changes from one isomer to another.

The absence of *cis-o*ES in the expansion keeps us from spectroscopically characterizing the isomer that is the likely direct precursor to any thermal rearrangement of ethynylstyrene to naphthalene. The absence of *cis-o*ES is a result of two factors. First, as mentioned previously, the *cis-ortho* isomer is predicted by DFT (B3LYP/6-31+G*) calculations to be higher in energy than trans by 8.33 kJ/mol. At room temperature, this energy difference results in a (preexpansion) Boltzmann population of the cis isomer that is only 5% of that of the trans isomer. Equally important, the barrier height out of the *cis-ortho* well is only 8.49 kJ/mol (710 cm^{-1}), a value sufficiently small that the isomerizing populations can partially reequilibrate to the low temperatures attained early in the expansion, further favoring trans over cis. A simple calculation illustrates why this is the case. In *o*ES, the average internal energy of the molecule at the nozzle temperature (50 °C) is ~1600 cm^{-1}. At that energy, RRKM theory provides an estimate for the *cis* → *trans* isomerization rate of $k_{isom}(E{=}1600 \text{ cm}^{-1}) \sim 1 \times 10^{11} \text{ s}^{-1}$. At the preexpansion backing pressure of 3 bar, the collision rate ranges from 4×10^9 to 4×10^7 s^{-1} as the distance from the nozzle varies from $x/D = 1-5$, respectively. As long as isomerization is fast compared to the collision rate (as the

preceding calculation suggests), the *cis* population will drain away to *trans* as the cooling proceeds.

Even though the difference in the relative energies of the *cis* and *trans* conformers of *o*ES is sufficient to make one isomer dominate over the other in the expansion, it is a very small difference relative to the energy of naphthalene, which is more stable than either isomer by about 250 kJ/mol. In the ground state, DFT (B3LYP/6-31G) calculations predict that the rate-limiting barrier for isomerization of *cis*-*o*ES to naphthalene is about 130 kJ/mol.[9] Further experimental and theoretical studies of the thermal rearrangement of *o*ES to naphthalene are needed before a final assessment can be made of this pathway as a route to naphthalene in combustion.

The conformation-specific spectroscopy presented here also clears up a puzzling result from earlier photochemical studies of the reaction of metastable diacetylene (C_4H_2*) with styrene.[10] That study identified $C_{10}H_8$ as an important product. Furthermore, based on one-color R2PI experiments, this $C_{10}H_8$ product was identified as *m*-ethynylstyrene by comparison of the product spectrum with the spectrum of a synthesized sample of *m*ES. However, based on the present work involving synthesized samples of all three isomers, it was determined that *m*- and *o*-ES isomers have S_0-S_1 transitions that are less than half way to the ionization potential, requiring two-color R2PI with a shorter wavelength photon in the ionization step (266 nm in this case). In the photochemical study, positive identification was made based on the correspondence of the photochemical product 1C-R2PI spectrum with a synthesized sample of *m*-ES. However, in the present work, all three isomers were synthesized independently. It is now clear (based on the spectra in Figures 3 and 4) that the 1C-R2PI spectrum in the C_4H_2* + styrene reaction was *p*ES present as an impurity in the *m*ES sample used in that work. Since 2C-R2PI spectra of the photochemical products were not carried out, it is likely that the previous study was "blind" to the *m*ES and *o*ES isomers. On that basis, we anticipate that all three isomers of ES will be produced as photoproducts of the C_4H_2* + styrene reaction.

B. The Nature of the Excited States. The present study of the ultraviolet spectroscopy of the ethynylstyrene isomers completes a series of substituted aromatics that includes all singly and doubly substituted vinyl and ethynyl substituents, including phenylacetylene (PA),[32,34] styrene (STY),[30,32] the *o*-, *m*-, and *p*-diethynylbenzenes (DEB),[21] two *meta* and one *para* isomer of the divinylbenzenes (DVB),[36] and now one *o*-, two *m*-, and one *p*-ethynylstyrene isomer (ES). Unlike many other substituents, both the vinyl and ethynyl substituents are conjugated with the phenyl ring, and therefore perturb and modify the π orbitals in significant ways. The ethynyl substituent is linear, and therefore preserves the C_2 symmetry axis in PA. This is not the case in STY, since the vinyl substituent is off-axis. It is a natural question to ask, then, whether one of the substituents in the ES isomers plays a more dominant role in perturbing the S_0 and S_1 states than the other. That is, is the $S_1 \leftarrow S_0$ transition more like that in styrene and phenylacetylene, or is it instead a unique mixture of the two? The answer to this question depends on what aspect of the spectroscopy is being probed.

1. The Electronic Frequency Shifts of the S_0-S_1 Origins. There is a clear pattern in the electronic frequency shifts of the $S_1 \leftarrow S_0$ origins in STY, PA, DEB, ES, and DVB. The parent molecule, benzene, has a (forbidden) $S_1 \leftarrow S_0$ origin at 38 085 cm^{-1}.[48] The addition of a vinyl group to make STY shifts this origin to the red by 3325 cm^{-1}, while the analogous substitution of an ethynyl group to form PA induces a red shift of 2206 cm^{-1}. Successive substitutions of a second vinyl or ethynyl group to form one of the DEB, ES, and DVB isomers produces further shifts that are of roughly the same magnitude. The precise wavenumber shifts depend on the position of substitution, with the meta isomers having values that are closest to additive (STY $\rightarrow$ *cis,cis-m*-DVB, $\Delta\nu = 3351$ cm^{-1}; PA $\rightarrow$ *cis-m*-ES, $\Delta\nu = 3196$ cm^{-1}; STY $\rightarrow$ *cis-m*-ES, $\Delta\nu = 2077$ cm^{-1}; PA $\rightarrow$ *m*-DEB, $\Delta\nu = 2073$ cm^{-1}). This rough additivity in shifts suggests that the two substituents produce independent effects on the ground and first excited singlet states of the molecules. However, one must be careful in inferring independence of the substituents based on the electronic frequency shift alone, since recent calculations by Bardeen and co-workers[49,50] have noted substantial coupling between *meta* substituents of the diethynylbenzenes in the first excited singlet state.

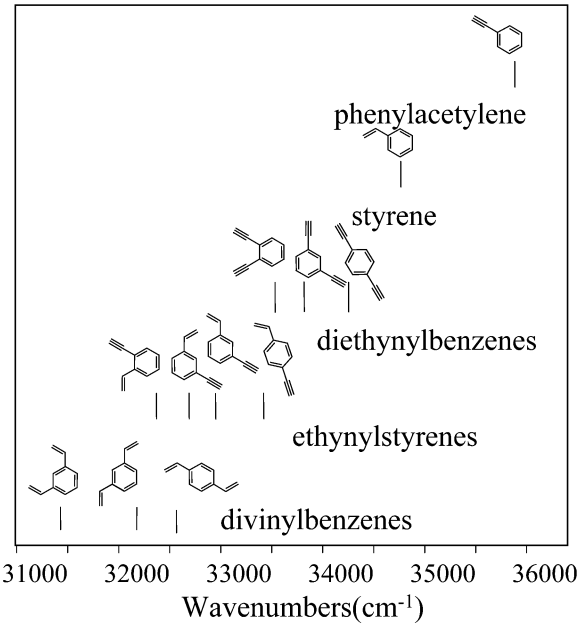

Figure 10. Electronic origin shifts of phenylacetylene, styrene, diethynylbenzenes, ethynylstyrenes, and divinylbenzenes.

However, as Figure 10 shows, there is also a clear trend in the positions of the electronic origins between isomers of a given molecule, indicating that the position and relative orientation of the two substituents also influences the S_0-S_1 separation. The largest shift occurs for the ortho isomer, intermediate for *meta*, and smallest for *para* substitution. Furthermore, in isomers involving the vinyl group, the *cis-meta* isomers have larger shifts than *trans-meta*. Qualitatively, we conclude that the magnitude of the red shift increases as the two substituents come closer together.

CIS calculations with a 6-31G basis set do not predict the trends in the S_0-S_1 origin shifts observed between the *ortho*, *meta*, and *para* isomers of a single system, nor do they predict the trends observed between the different monosubstituted and disubstituted systems that are shown in Figure 10. This failure of the CIS method is not surprising given the lack of electron correlation in these calculations.

2. The Direction of the Transition Dipole Moment. One of the principal outputs from fitting the rotational structure in the S_0-S_1 origin transition is the direction of the transition dipole moment. In simple unconjugated substituted benzenes, the direction of the S_0-S_1 transition moment depends sensitively on the degree to which the substituent creates asymmetry in the benzene ring. This has been used as a diagnostic of the conformation of the phenyl ring side chain.[51] In the ethynylstyrenes, the ethynyl and vinyl groups are both conjugated with

the ring, and their π/π^* orbitals play a more active role in mixing with the phenyl ring π/π^* orbitals. Such mixing can lead to differences in the transition moments that are difficult to understand *via* simple arguments. For instance, the direction of the transition moment swings almost 90° in going from STY (*a*-axis polarized) to PA (*b*-axis polarized), as shown in Figure 2a.[32]

On one level, we can simply use the direction of the transition moment as a diagnostic of the relative roles of the ethynyl and vinyl groups in the S_1 states of the ES isomers. Direct determinations of S_0-S_1 transition moment directions are available for three isomers of DVB[36] (Figure 2b) and three isomers of ES (Figure 2c). Less direct arguments based on vibronic coupling have provided tentative assignments for the transition moments of the three isomers of DEB (Figure 2d).[21,35] In Figure 2, the transition moment direction is labeled both with the inertial axis and with the Platt designations for the state (^1L_a and ^1L_b). All the ethynyl- and vinyl-disubstituted isomers studied to date have "*a*"-axis polarized S_0-S_1 transitions except for *p*-DEB, which is "*b*"-axis polarized (Figure 2).

The prediction based on STY and PA is that the vinyl group tends to direct the S_0-S_1 transition moment toward the position of substitution (*a*-axis), whereas the ethynyl group directs it perpendicular to this direction (*b*-axis). This prediction is borne out by *p*DVB ("*a*"-axis polarized, Figure 2b) and *p*DEB ("*b*"-axis polarized, Figure 2d). The case of *p*ES is especially interesting, because it combines the ethynyl and vinyl groups, with their opposing effects, in the same molecule. The experimental determination that the S_0-S_1 origin transition of *p*ES is primarily "*a*"-axis polarized suggests that the vinyl group plays a dominant role in determining the direction of the transition moment. A simple interpretation of this result is that the vinyl group's π/π^* orbitals mix more strongly with the phenyl ring π/π^* orbitals than do the ethynyl group, in keeping with the closer energetic proximity of the vinyl group's orbitals to those of the phenyl ring.[52]

On the other hand, the *meta*-substituted species all have transition moments that are "*a*"-axis polarized, despite the fact that a naïve application of the directing propensities of the substituents would predict mixed bands with substantial "*b*"-axis character. This suggests that the relative position of the two groups on the ring plays an equally important role to the nature of the substituent in determining the transition moment direction.

It is perhaps not surprising that CIS (6-31G) calculations do not predict the excited states of the ethynylstyrenes with sufficient accuracy to have any predictive power. As often as not, the CIS results also predict transition moment directions that are different from those measured experimentally. Furthermore, a simple swap of the first two excited states cannot correct the problem. The presence of the conjugated substituents produces molecular orbitals that are complicated mixtures of phenyl, vinyl, and ethynyl atomic orbitals. Furthermore, the excited states have contributions from several one-electron transitions beyond HOMO-LUMO that are not correctly described by CIS calculations.

These complications also carry over to the designations of the excited states. In unconjugated benzene derivatives, the first two excited states are sometimes labeled as ^1L_a and ^1L_b, with ^1L_b typically lower in energy than ^1L_a. Unfortunately, these designations have nothing to do with either the inertial axes or the symmetry designations of the molecule, leading to considerable confusion in their application. For our purposes here, it is only important to realize that these designations assume that the first two excited states have transition moments from the ground state that are perpendicular to one another, with one pointing along the "*a*" axis (not necessarily ^1L_a!), while the other points along the "*b*" axis. The $^1L_a/^1L_b$ designations are placed alongside the inertial axes in Figure 2.[53] As Ribblett *et al.*[32] and Nguyen *et al.*[36] have noted, the off-axis nature of the vinyl substituent breaks the C_2 symmetry about the $C_\phi-C_\alpha$ bond. Furthermore, the conjugated nature of the vinyl and ethynyl substituent stretches well beyond the original model proposed by Platt, which involved simple concatenated benzenes and their unconjugated derivatives. Even at the CIS level of theory, the result is that the first two excited states no longer have transition moments that are necessarily perpendicular to one another, so that the entire foundation for the $^1L_a/^1L_b$ designations is on less firm ground in this context.

3. Vibronic Structure. The vibronic structure can serve as an additional spectroscopic probe of the contributions of the vinyl and ethynyl groups to the S_1 excited states of the ES isomers. The observed Franck−Condon activity reflects the structural change accompanying electronic excitation. In principle, the assignment and fitting of the Franck−Condon progressions can be used to quantify these structural changes, as has recently been demonstrated for benzonitrile, cyanophenol, chlorobenzene, and chlorophenol by Imhof *et al.*[54] A thorough analysis of this type must await single vibronic-level dispersed fluorescence spectra. However, certain elements of the vibronic structure are readily assigned based on a comparison with similar molecules, as has been discussed in Section IV.

Three aspects of these assignments deserve special mention. First, the strong vibrational progressions in the ES isomers are those common to all benzene derivatives, involving modes that correlate with ν_{6a}, ν_1, ν_{12}, and ν_{13} in benzene. This indicates that the major structural changes in the ring are similar to those in most unconjugated benzene derivatives. Second, among the three structural isomers, only *o*ES shows clear evidence for strong vibronic coupling to the S_2 state. In this sense, *o*ES shares much in common with PA and the DEB isomers, suggesting that the ethynyl group is playing a more active role in the spectroscopy of the *ortho* isomer. Finally, the R2PI spectra of the *meta* and *para* isomers clearly show low-frequency vibronic structure in the 230−350 cm^{-1} region that likely arises from the vinyl group torsional mode, much as appears in STY. The *ortho* isomer does not show these bands built off the weak S_0-S_1 origin, but the false origins at 384 and 421 cm^{-1} that appear from vibronic coupling with S_2 do show such activity built off of them. This suggests that the S_2 state of *o*-ES may involve substantial vinyl participation that is transmitted to the S_1 state via vibronic coupling that is mediated primarily by the ethynyl group. In summary, vibronic coupling in the *ortho* isomer appears to be a signature of the ethynyl group participation in the transition, while the torsional Franck−Condon activity reflects the effect of the vinyl group.

C. The Isomerization Barrier in *m*-Ethynylstyrene. A unique aspect of the present study is the application of a new method, namely, SEP-population transfer spectroscopy, to directly measure the energy thresholds for *cis* → *trans* and *trans* → *cis* isomerization in *m*ES. This method has been used recently to measure the energy thresholds for isomerization in tryptamine (which possesses seven conformations and several flexible degrees of freedom),[11,55] 3-indole propionic acid (IPA) and IPA−H_2O,[56] and *trans*-formanilide-H_2O.[57]

Table 5 summarizes the relative energies of *cis*-*m*ES and *trans*-*m*ES and the barrier to isomerization determined by using this method, together with comparisons to DFT calculations and

TABLE 5: Relative Energies and Barriers to *Cis*−*Trans* Isomerization in Styrene and *m*-ethynylstyrene

	rel energy (cm^{-1})	
compd	exptl	calcd
cis-m-ethynylstyrene	−75 to +81[a]	+29[c]
	barrier to *cis*−*trans* isomerization (cm^{-1})	
compd	exptl	calcd
m-ethynylstyrene	990−1070[a]	1237[c]
styrene	1070 ± 8[b]	1350[c]

[a] This work. [b] Reference 12. [c] B3LYP/6-31+G* with ZPE correction.

to previous results on styrene. The barrier to isomerization in *m*ES is only slightly lower than that in STY, indicating the presence of the ethynyl group has little effect on the isomerization of the vinyl group. The insensitivity of the vinyl group barrier to the presence of the ethynyl group in the *meta* position suggests that conjugation between the two substituents is not important in the meta isomer. In both STY and *m*ES, DFT calculations overestimate the barrier by ∼15−25%. The relative energies of the *cis* and *trans* minima ($-75 \le E(cis) - E(trans) \le +81$ cm^{-1}) in the ground electronic state of *m*ES are consistent with calculations and the approximately equal observed intensities of the origin bands in the R2PI spectrum.

The isomerization barrier in styrene was calculated by Hollas and co-workers by fitting the C(1)−C(α) torsional levels, ν_{42}, to the torsional potential function:[12]

$$V(\varphi) = {}^1/_2\sum V_n(1 - \cos n\,\varphi)$$

The majority of the torsional levels were determined from SVL dispersed emission scans, with confirming evidence from gas-phase absorption spectra[30] and Raman spectra.[58] The best fit of the experimental data was achieved with the following functional form:[12]

$$V(\varphi)/\mathrm{cm}^{-1} = {}^1/_2[(1070 \pm 8)(1 - \cos 2\varphi) - (275 \pm 1)(1 - \cos 4\varphi) + (7 \pm 0.5)(1 - \cos 6\varphi)$$

The value of the torsional barrier height (1070 ± 8 cm^{-1}) in this potential is determined by the V_2 term. Such fitting is particularly powerful because it gives not only the height of the barrier, but also the precise shape of the entire potential energy function along the torsional coordinate. This method has been successfully applied to determine torsional potentials for the vinyl group in *o*-, *m*-, and *p*-fluorostyrene[38,39,42] and *p*-methylstyrene.[41]

Despite the power of the method, it also has certain limitations as a general method of determining isomerization barrier heights. First, the method relies on direct spectroscopic detection of vibrational levels associated with the reaction coordinate, the torsional coordinate of the vinyl group in this case. If the coordinate of interest is not Franck−Condon active, the method fails. Second, connecting the torsional potential with the isomerization barrier necessitates equating the torsional coordinate with the isomerization reaction coordinate. However, in principle, the vinyl group could also flex along other coordinates as it rotates through the perpendicular configuration. The optimized (B3LYP/6-31+G*) transition state structure for *cis-m*ES → *trans-m*ES isomerization has the vinyl group 90.8° out of the plane of the ring, as one would anticipate if the vinyl torsion closely approximates the reaction coordinate. However, there are also changes in other coordinates, most notably an increase in the C(1)−C(α) bond length (1.475 Å to 1.492 Å) and the ring CCC angles becoming larger parallel to the point of substitution of the vinyl group. In other more complicated isomerization reactions, no single normal mode will map onto the reaction coordinate. Finally, the torsional levels probed directly in the spectroscopy are still well below the top of the barrier. As a result, a long extrapolation is necessary in the fitted potential.

The SEP-PT method directly measures the energy threshold by looking for the first appearance of population transfer from the selectively excited "reactant" isomer to the "product" isomer of interest. The SEP step does not rely on excitation of a particular torsional level, but rather uses the SEP "dump" step to place a well-defined amount of energy in a particular isomer. In its most basic form, the SEP-PT spectrum asks a simple "yes/no" question regarding the threshold to isomerization. If the energy is below the barrier to isomerization, no isomerization will occur; if it is above, isomerization can occur, producing an increase in population of the product isomer. In this way, SEP-PT spectroscopy provides a direct and sensitive means of measuring isomerization barrier heights. Furthermore, by viewing the isomerization as a specific reactant → product direction, a series of measurements can be pieced together to determine the relative energies of the minima as well.

Admittedly, the SEP-PT method also has its limitations. The accuracy with which the barrier height is determined depends on the spacing and intensity of the transitions in the SEP spectrum. If the spectrum is sparse, it leads to large uncertainties in the barrier to isomerization. Furthermore, the observation of population transfer relies on detecting a difference in population of a particular isomer with and without the SEP dump laser present. In circumstances where the reactant → product isomer pair studied involves a reactant isomer with small population, this population change can be difficult to observe. Finally, the population transfer relies on isomerization occurring on a time scale that can successfully compete with collisional cooling. In principle, this could lead to a kinetic shift in the observed isomerization threshold.

In fact, the SEP-PT spectra of Figure 9b,d do show evidence for this competition in the reduced intensity of the first observed transition near 990 cm^{-1}. A simple RRKM estimate of the isomerization rate at threshold is 2.6×10^9 s^{-1} for cis−trans and 2.5×10^9 s^{-1} for trans−cis isomerization. By comparison, under the conditions of the SEP-PT spectrum ($x/D = 2$, $P_0 =$ 4 bar), we estimate a collision rate of *m*ES with helium of 1×10^9 s^{-1}. At threshold (∼1000 cm^{-1}), each collision should remove a few wavenumbers of internal energy from *m*ES ($\Delta E/E = 0.003$).[59] This suggests that isomerization should successfully compete with collisional cooling, even at threshold. On this basis, we would conclude that the reduced intensity of the 990-cm^{-1} band in the SEP-PT spectrum is probably because this band just happens to be right at the threshold for the isomerization. However, this estimate is based on several assumptions that need further scrutiny, calling for more systematic and quantitative studies of the SEP-PT intensities as a function of energy and collisional cooling rate.[60]

As the results in Table 5 show, the methods of SEP-PT spectroscopy and torsional potential fitting yield essentially indistinguishable values for the barrier height in *m*ES and STY. This provides a consistency check on both methods and bodes well for the application of SEP-PT spectroscopy to the determination of isomerization barrier heights in a much wider variety of circumstances where other methods fail. Furthermore, careful

study of the intensities near threshold holds promise for determining the rates of isomerization in large flexible molecules.

Acknowledgment. The authors thank Alexei Nikolaev and John Yi for their assistance and gratefully acknowledge the support of the Department of Energy Basic Energy Sciences, Division of Chemical Sciences under Grant No. DE-FG02-96ER14656 (T.S.Z.) and the National Science Foundation Grant No. CHE-0315584 (D.W.P.).

Supporting Information Available: The detailed syntheses of all three *x*-ethynylstyrenes ($x = 2, 3, 4$) and their analysis data. This material is available free of charge via the Internet at http://pubs.acs.org.

References and Notes

(1) Roubaud, A.; Lemaire, O.; Minetti, R.; Sochet, L. R. *Combust. Flame* **2000**, *123*, 561.
(2) Tancell, P. J.; Rhead, M. M.; Pemberton, R. D.; Braven, J. *J. Fuel* **1996**, *75*, 717.
(3) Pope, C. J.; Miller, J. A.; Homann, K. H.; Kohse-Hoinghaus, K. *Proc. Combust. Inst.* **2000**, *28*, 1519.
(4) Westbrook, C. K.; Pitz, W. J.; Boercker, J. E.; Curran, H. J.; Griffiths, J. F.; Mohamed, C.; Ribaucour, M. *Proc. Combust. Inst.* **2003**, *29*, 1311.
(5) Miller, J. A.; Klippenstein, S. J. *J. Phys. Chem. A* **2001**, *105*, 7254.
(6) Bedanov, V. M.; Tsang, W.; Zachariah, M. R. *J. Phys. Chem.* **1995**, *99*, 11452.
(7) Frenklach, M. *Phys. Chem. Chem. Phys.* **2002**, *4*, 2028.
(8) Lindstedt, P.; Maurice, L.; Meyer, M. *Faraday Discuss.* **2002**, *119*, 409.
(9) Prall, M.; Krüger, A.; Schreiner, P. R.; Hopf, H. *Chem. Eur. J.* **2001**, *7*, 4386.
(10) Robinson, A. G.; Winter, P. R.; Zwier, T. S. *J. Phys. Chem. A* **2002**, *106*, 5789.
(11) Dian, B. C.; Clarkson, J. R.; Zwier, T. S. *Science* **2004**, *303*, 1169.
(12) Hollas, J. M.; Musa, H.; Ridley, T.; Turner, P. H.; Weisenberger, K. H.; Fawcett, V. *J. Mol. Spectrosc.* **1982**, *94*, 437.
(13) Takahashi, S.; Kuroyama, Y.; Sonogashira, K.; Hagihara, N. *Synthesis* **1980**, 627.
(14) Maeyama, K.; Iwasawa, N. *J. Org. Chem.* **1999**, *64*, 1344.
(15) Tsuda, K.; Miyajima, M.; Kakuchi, T.; Yokota, K. *Kenkyu Hobun−Asahikawa Kogyo Koto Senmon Gakko* **1992**, *29*, 117.
(16) Austin, W. B.; Bilow, N.; Kelleghan, W. J.; Lau, K. S. Y. *J. Org. Chem.* **1981**, *46*, 2280.
(17) Aubert, C.; Gotteland, J. P.; Malacria, M. *J. Org. Chem.* **1993**, *58*, 4298.
(18) Greene, T. W.; Wuts, P. G. M. *Protective Groups in Organic Synthesis*, 3rd ed.; John Wiley & Sons: New York, 1999.
(19) Arrington, C. A.; Ramos, C.; Robinson, A. D.; Zwier, T. S. *J. Phys. Chem. A* **1998**, *102*, 3315.
(20) Page, R. H.; Shen, Y. R.; Lee, Y. T. *J. Chem. Phys.* **1988**, *88*, 5362.
(21) Stearns, J. A.; Zwier, T. S. *J. Phys. Chem. A* **2003**, *107*, 10717.
(22) Majewski, W. A.; Pfanstiel, J. F.; Plusquellic, D. F.; Pratt, D. W. *Laser Techniques in Chemistry*; Wiley: New York, 1995.
(23) Plusquellic, D. F. To be submitted for publication.
(24) Becke, A. D. *Phys. Rev. Sect. A* **1988**, *38*, 3098.
(25) Lee, C.; Yang, W.; Parr, R. G. *Phys. Rev. Sect. B* **1988**, *37*, 785.
(26) Frisch, M. J.; Pople, J. A.; Binkley, J. S. *J. Chem. Phys.* **1984**, *80*, 3265.
(27) Peng, C.; Schegel, H. B. *Isr. J. Chem* **1993**, 449.
(28) Foresman, J. B.; Head-Gordon, M.; Pople, J. A.; Frisch, M. J. *J. Phys. Chem.* **1992**, *96*, 135.
(29) Frisch, M. J.; Trucks, G. W.; Schlegel, H. B.; Scuseria, G. E.; Robb, M. A.; Cheeseman, J. R.; Zakrzewski, V. G.; Montgomery, J. A., Jr.; Stratmann, R. E.; Burant, J. C.; Dapprich, S.; Millam, J. M.; Daniels, A. D.; Kudin, K. N.; Strain, M. C.; Farkas, O.; Tomasi, J.; Barone, V.; Cossi, M.; Cammi, R.; Mennucci, B.; Pomelli, C.; Adamo, C.; Clifford, S.; Ochterski, J.; Petersson, G. A.; Ayala, P. Y.; Cui, Q.; Morokuma, K.; Malick, D. K.; Rabuck, A. D.; Raghavachari, K.; Foresman, J. B.; Cioslowski, J.; Ortiz, J. V.; Stefanov, B. B.; Liu, G.; Liashenko, A.; Piskorz, P.; Komaromi, I.; Gomperts, R.; Martin, R. L.; Fox, D. J.; Keith, T.; Al-Laham, M. A.; Peng, C. Y.; Nanayakkara, A.; Gonzalez, C.; Challacombe, M.; Gill, P. M. W.; Johnson, B. G.; Chen, W.; Wong, M. W.; Andres, J. L.; Head-Gordon, M.; Replogle, E. S.; Pople, J. A. *Gaussian 98*, Revision A.7; Gaussian, Inc.: Pittsburgh, PA, 1998.
(30) Hollas, J. M.; Khalilipour, E.; Thakur, S. N. *J. Mol. Spectrosc.* **1978**, *73*, 240.
(31) Hollas, J. M.; Ridley, T. *Phys. Chem. Lett.* **1980**, 94.
(32) Ribblett, J. W.; Borst, D. R.; Pratt, D. W. *J. Chem. Phys.* **1999**, *111*, 8454.
(33) Hollas, J. M.; Ridley, T. *J. Mol. Spectrosc.* **1981**, *89*, 232.
(34) King, G. W.; So, S. P. *J. Mol. Spectrosc.* **1971**, *37*, 543.
(35) Laposa, J. D. *J. Lumin.* **1979**, *20*, 67.
(36) Nguyen, T. V.; Ribblett, J. W.; Pratt, D. W. *Chem. Phys.* **2002**, *283*, 279.
(37) Hollas, J. M.; Bin Hussein, M. Z. *J. Mol. Spectrosc.* **1989**, *136*, 31.
(38) Hollas, J. M.; Bin Hussein, M. Z. *Chem. Phys. Lett.* **1989**, *154*, 14.
(39) Hollas, J. M.; Bin Hussein, M. Z. *Chem. Phys. Lett.* **1989**, *154*, 228.
(40) Hollas, J. M.; Bin Hussein, M. Z. *J. Mol. Spectrosc.* **1989**, *135*, 59.
(41) Hollas, J. M.; Taday, P. F. *J. Mol. Spectrosc.* **1992**, *153*, 587.
(42) Hollas, J. M.; Bin Hussein, M. Z. *J. Mol. Spectrosc.* **1991**, *145*, 89.
(43) Mulliken, R. S. *J. Chem. Phys.* **1953**, *23*, 1997.
(44) Wilson, E. B. *Phys. Rev.* **1934**, *45*, 706.
(45) Syage, J. A.; Adel, F. A.; Zewail, A. H. *Chem. Phys. Lett.* **1983**, *103*, 15.
(46) Nyquist, R. A.; Potts, W. J. *Spectrochim. Acta* **1960**, *16*, 419.
(47) King, G. W.; So, S. P. *J. Mol. Spectrosc.* **1970**, *36*, 468.
(48) Stephenson, T. A.; Rice, S. A. *J. Chem. Phys.* **1984**, *81*, 1073.
(49) Gaab, K. M.; Thompson, A. L.; Xu, J.; Martinez, T. J.; Bardeen, C. J. *J. Am. Chem. Soc.* **2003**, *125*, 9288.
(50) Thompson, A. L.; Gaab, K. M.; Xu, J.; Bardeen, C. J.; Martinez, T. J. *J. Phys. Chem. A* **2004**, *108*, 671.
(51) Kroemer, R. T.; Liedl, K. R.; Dickinson, J. A.; Robertson, E. G.; Simons, J. P.; Borst, D. R.; Pratt, D. W. *J. Am. Chem. Soc.* **1998**, *120*, 12573.
(52) HF calculations show that the HOMO of ethylene (−10 eV) is higher and closer in energy to benzene's HOMO (−9 eV) than the HOMO of acetylene (−11 eV). Likewise, the LUMO of ethylene (5 eV) is lower and closer in energy to the LUMO of benzene (4 eV) than the LUMO of acetylene (6 eV). As a result, the mixing of the HOMO and LUMO of benzene with the HOMO and LUMO of the vinyl group should be greater than that for the ethynyl group.
(53) According to Platt's original definition (Platt, J. R. *J. Chem. Phys.* **1949**, *17*, 484), "for hexagonal ring systems, when some bonds are just parallel or perpendicular to a symmetry axis, the ^{1}A-^1L_a moment will be parallel to these bonds, the ^{1}A-^1L_b moment perpendicular." This definition is insufficient in cases where there is more than one symmetry axis, as can occur in disubstituted benzenes (e.g., *p*-diethynylbenzene). The functional definition of ^1L_a and ^1L_b in the case of substituted benzenes is simply to focus on the direction of the transition moment in the phenyl ring. Transition moments that intersect atoms on the ring are called ^1L_a while transition moments that intersect bonds are called ^1L_b. In principle, this definition can hold no matter what the substitution. In practice, when there is more than one substituent and when the substituents asymmetrize the ring, the transition moment can take on directions anywhere in the plane, and thus cannot as easily be assigned as through atom or through bond.
(54) Imhof, P.; Krugler, D.; Brause, R.; Kleinermanns, K. *J. Chem. Phys.* **2004**, *121*, 2598.
(55) Clarkson, J. R.; Dian, B. C.; Moriggi, L.; DeFusco, A.; McCarthy, V.; Jordan, K. D.; Zwier, T. S. *J. Chem. Phys.* **2005**, in press.
(56) Clarkson, J. R.; Baquero, E.; Zwier, T. S. *J. Chem. Phys.* **2005**, in press.
(57) Clarkson, J. R.; Baquero, E.; Shubert, V. A.; Myshakin, E.; Jordan, K. D.; Zwier, T. S. *Science* **2005**, *307*, 1443.
(58) Carreira, L. A.; Towns, T. G. *J. Chem. Phys.* **1975**, *63*, 5283.
(59) The amount of energy removed, on average, per collision with helium is not known with any accuracy. However, previous estimates in larger molecules suggested that about 0.3% of the internal energy of a molecule was removed per collision with helium.
(60) Leitner, D. M.; Levine, B.; Quenneville, J.; Martinez, T. J.; Wolynes, P. G. *J. Phys. Chem. A* **2003**, *107*, 10706.